Corrected 23 December 2011; see below

www.sciencemag.org/cgi/content/full/science.1211222/DC1

Supporting Online Material for

Mouse B-Type Lamins Are Required for Proper Organogenesis But Not by Embryonic Stem Cells

Youngjo Kim, Alexei A. Sharov, Katie McDole, Melody Cheng, Haiping Hao, Chen-Ming Fan, Nicholas Gaiano, Minoru S. H. Ko*, and Yixian Zheng*

*To whom correspondence should be addressed. E-mail: zheng@ciwemb.edu (Y.Z.); KoM@grc.nia.nih.gov (M.S.H.K.)

Published 24 November 2011 on *Science* Express
DOI: 10.1126/science.1211222

This PDF file includes

Materials and Methods
Figs. S1 to S19
Tables S2 to S7
References

Other Supporting Online Material for this manuscript includes the following:
(available at www.sciencemag.org/cgi/content/full/science.1211222/DC1)

Table S1. Lamin-B1 binding to promoters of genes in mouse ESCs and TE cells.

Correction: A new reference 26 has been added, and former references 26 to 34 and their citations have been renumbered 27 to 35.

Materials and Methods

ESC and TE cell culture and differentiation

ZHBTc4 ESCs were maintained in complete GMEM medium [10% fetal bovine serum (FBS, Invitrogen), 100 μM β-mercaptoethanol (Invitrogen), 2 mM L-glutamine, 0.1 mM nonessential amino acids, 1 mM sodium pyruvate, 50 μg/ml penicillin/streptomycin, and 1,000 units/ml LIF (Millipore) in GMEM (Invitrogen)]. The protocol for differentiation of trophectoderm lineage (TE) cells from ZHBTc4 ESCs via trophoblast stem cells (TSC) was modified from published protocols *(21, 27)*. Briefly, to establish TSC, ZHBTc4 ESCs cultured in the absence of tetracycline were plated at 1.2 x 10^4 cells/cm^2 in a culture dish containing 30% TS medium (20% FBS, 1mM sodium pyruvate, 2 mM L-glutamine, 100 μM β-mercaptoethanol, 50 μg/ml penicillin/streptomycin in RPMI1640), 70% FCM (fibroblast conditioned medium, *i.e.*, the supernatant of mitomycin-treated MEF cultured in TS medium), 100 nM FGF4 (Peprotech, 100-31), 1 μg/ml heparin (Sigma, H3149) and 1 μg/ml tetracycline (Sigma, T7660). Medim was changed every 48 hours until the typical TSC morphology. The TSCs were than passaged for 3~4 times and frozen. TE cells were obtained by culturing the TSC in 100% TS medium for 6 days. Although TE cells can be differentiated directly from ZHBTc4 ESC by adding tetracycline, differentiation from the ZHBTc4-derived TSCs resulted in more efficient terminal TE lineage differentiation. ZHBTc4 ESCs, TSCs, and TE cells were cultured in the absence of feeder cells.

Plasmid construction and antibody production

To generate the Dam-*Lmnb1* (mouse lamin-B1) construct, mouse *Lmnb1* cDNA was amplified from IMAGE clone #6816118 with primers carrying Gateway recombination sequences. The PCR product was cloned into pDONR201, and subsequently into pLgwEcoDamV5 (*28*). The resulting construct, pLgwEcoDamV5-*Lmnb1,* was confirmed by DNA sequencing. pLgwV5EcoDam was used as the Dam control construct. To raise the lamin-B2 specific antibody, cDNA sequence encoding the Ig-fold domain (383-596 amino acids) of mouse lamin-B2 protein was amplified from IMAGE clone #5696459, cloned into pET28a expression vector, expressed, purified, and injected into chickens. IgY specific for lamin-B2 was affinity purified from the eggs using the lamin-B2 antigen. To express Histone H2B-GFP in ESCs, the H2B-GFP sequence was obtained by digesting pBOS H2B-GFP-N1 (BD Pharmingen) with SalI/NotI and cloned into the XhoI/NotI sites of pPyCAGIP. pLgwEcoDamV5 and pLgwV5EcoDam vectors were gifts from Dr. B. van Steensel. pPyCAGIP vector was generously provided by Dr. H. Niwa.

DamID analyses of lamin-B1 and chromatin interactions in ESCs and TE cells

DamID was performed as described (*28*) with modifications. Briefly, the Dam and Dam-*Lmnb1* lentivirus generated from 293T cells was concentrated by centrifuging at 25,000 rpm with an SW28Ti rotor (Beckman) for 3 hours. The virus pellets were resuspended in PBS. For ESCs, freshly trypsinized ESCs were plated into a 6-well plate with 2 ml complete GMEM medium containing either Dam or Dam-lamin-B1 lentivirus, spin-infected at 700g for 45 min, and incubated at 37^{o}C for a total of 48 hours. For TE cells, TSCs were differentiated toward TE cells for 6 days. On day 6, the TE cells were

transduced by spin-infection as above with fresh TS medium containing either Dam or Dam-*Lmnb1* lentivirus and incubated at 37°C for 48 hours. The adenine-methylated DNAs were amplified from the genomic DNA by adaptor mediated PCR and labeled using a Dual color DNA labeling kit (Roche). The labeled DNA was hybridized according to the manufacturer's recommendations to 2.1M mouse whole-genome tiling arrays (NimbleGen # 05327911001), which covers the entire genome at approximately 250 bp intervals.

DamID data analysis

Microarray data were dye-normalized using broken line interpolation of log-transformed data ($\log_{10}$) at intervals of 0.2. The extent of lamin-B1 binding in each location is measured by the log-ratio of red intensity (Dam-*Lmnb1*) to green intensity (Dam alone). Genome locations were converted from the mm8 version of mouse genome (used for tiling array design) to the current mm9 version using the UCSC batch conversion tool (http://genome.ucsc.edu/cgi-bin/hgLiftOver). However, we used original genome coordinates (mm8) for the analysis of lamin-B1 binding in Long terminal repeats (LTRs) and Long interspersed nuclear elements (LINEs) because the conversion tool is not reliable in repetitive regions. To analyze lamin-B1 binding at specific regulatory regions, we estimated the average $\log_{10}$ ratio for all genome locations that matched selected criteria (e.g., distance from TSS or transcription factor binding site). Different array features were used as replications to estimate standard error (SE).

Generation of *Lmnb1* and *Lmnb2* knock out mice

DNA fragments for homologous recombination arms of *Lmnb1* and *Lmnb2* targeting vectors were amplified from C57BL/6J mouse BAC clones RP23-208A22 and RP23-382P20, respectively. Primers for the 5' 2.0 kb arm of *Lmnb1* were 5'-CAG AGC GAT CGC TGG ATT TGG AAA ACA ACT CTG CGT GT-3' and 5'-CCA CAA GCT TTT AAT CAT TGG CTA TGA ACG CGG ATG-3'; primers for the 3' 4.0 kb arm of *Lmnb1* were 5'- CCA CTT AAT TAA TTT AGA ACT GAA CAG GGG TGC CTT GG-3' and 5'-CTC GGG CGC GCC AGT TCC TGA GTT CCT GAC TCG CTT CC-3'; primers for the 5' 2.0 kb arm of *Lmnb2* were 5'-CAG AGC GAT CGC TGG ATT TGG AAA ACA ACT CTG CGT GT-3' and 5'-CCA CAA GCT TTT AAT CAT TGG CTA TGA ACG CGG ATG-3'; primers for the 3' 4.0 kb arm of *Lmnb2* were 5'-CCA CTT AAT TAA TTT AGA ACT GAA CAG GGG TGC CTT GG-3' and 5'-CTC GGG CGC GCC AGT TCC TGA GTT CCT GAC TCG CTT CC-3'. The amplified fragments were sequentially cloned into pYZ1932, a gene-targeting vector containing PGK-Neo^R and HSV-*tk* (full information available upon request). The targeting vectors were linearized with AsiSI and electroporated into V6.5 mouse ESCs. After selection with 400 μg/ml G418 (Invitrogen) and 2 μM ganciclovir (Sigma, G2536), ESC clones were screened for homologous recombination by PCR of the flanking regions of the 5' and 3' recombination arms from the genomic DNA (Fig. S4). The PCR primers used to screen for the homologously recombined ESC clones are as follows:

5' arm of *Lmnb1* (a PCR fragment of 2,161 bp indicates homologous recombination)

pr66 5'-CCA CCA ATC CCA TTA TCA CGT GTG TA-3' (outside of the 5' recombination arm in the *Lmnb1* null allele)
pr67 5'-AGC TAG CTT GGC TGG ACG TAA ACT CC-3' (*Neo*^{R} specific)

3' arm of *Lmnb1* (a PCR fragment of 4,441bp indicates homologous recombination)
pr511 5'-ACG AGT TCT TCT GAG GGG ATC AAT TC-3' (*Neo*^{R} specific)
pr512 5'-ACT CTC CAA CAG TGT TCC TCC GCT CC-3' (outside of the 3' recombination arm in the *Lmnb1* null allele)

5' arm of *Lmnb2* (a PCR fragment of 2,211bp indicates homologous recombination)
pr102 5'-GTG CAG GGC AGT GTG AAT CAG ATA GG-3' (outside of the 5' recombination arm in the vector)
pr67 5'-AGC TAG CTT GGC TGG ACG TAA ACT CC-3' (*Neo*^{R} specific)

3' arm of *Lmnb2* (a PCR fragment of 4,463 indicates homologous recombination)
pr511 5'-ACG AGT TCT TCT GAG GGG ATC AAT TC-3' (*Neo*^{R} specific)
pr513 5'-GTG GCT TCT GGC AGT GGT TTC TGT AG-3' (outside of the 3' recombination arm in the vector)

Correctly targeted ESC clones were injected into CD1 blastocysts and male chimeras were mated with 129S6/SvEvTac females (Taconic) to produce germline transmitted offspring as described (*29*). The *Lmnb1* and *Lmnb2* mice were maintained as heterozygotes on a mixed genetic background (C57BL/6;129S4Sv/Jae;129S6/SvEvTac). Mice were genotyped by PCR using the following primer sets (Fig. S4):

Lmnb1 wt allele (623 bp PCR fragment)
pr107 5'-GGGTGACGAAGCAAAAACCTTGTCTC-3'
pr108 5'-CTCTCGTGGAACCCCGTGCGGACCCC-3'

Lmnb1 null allele (400 bp PCR fragment)
pr107 5'-GGGTGACGAAGCAAAAACCTTGTCTC-3'
pr67 5'-AGCTAGCTTGGCTGGACGTAAACTCC-3'

Lmnb2 wt allele (546 bp PCR fragment)
pr110 5'-TCTGTGTCACGGAGGTTGCCCTTGAG-3'
pr111 5'-GACGGGCTTTGGTTGGTCTCTGTTGG-3'

Lmnb2 null allele (228 bp PCR fragment)
pr110 5'-TCTGTGTCACGGAGGTTGCCCTTGAG-3'
pr67 5'-AGCTAGCTTGGCTGGACGTAAACTCC-3'

Derivation of embryonic stem cells

To derive lamin-B null ESCs, *Lmnb1* and *Lmnb2* double heterozygous mice (*Lmnb1*$^{+/-}$*Lmnb2*$^{+/-}$) were mated with each other. Blastocysts were flushed at 3.5 dpc using the standard technique. Isolated blastocysts were plated in pre-equilibrated N2B27 2i (*25*) or equivalent medium (Millipore, SF001-100P) and incubated at 37°C in a 7%

CO_2 tissue culture incubator. After 5 days, the vast majority of trophectoderm layers surrounding the inner cell mass (ICM) were removed by incubating with Accutase (Millipore, SF006) and pipetting vigorously with aspirator tube assemblies (Sigma, A5177) equipped with a micropipet (VWR, 53432-740). The isolated ICMs were individually transferred to fresh N2B27 2i medium and incubated at 37°C. After 5 days, the expanded ICMs were disaggregated into small cell clumps with Accutase and replated. The emerging ESC colonies were picked and genotyped for *Lmnb1, Lmnb2, Xist and Sry genes*. *Xist* and *Sry* genes, which are specific for X and Y chromosomes, respectively, were used to determine the sex of the ESCs. The PCR primers used are as follows:

Xist (566 bp PCR fragment)
5'-GCTTTGTTTCACTTTCTCTGGTGC-3'
5'-ATTCTGGACCTATTGGGAAGGGGC-3'

Sry (321 bp PCR fragment)
5'-GCATTTATGGTGTGGTCCCGTG-3'
5'-CCAGTCTTGCCTGTATGTGATGG-3'

After genotyping, the male ESCs were expanded on MEF feeder cells with ESC culture medium (15% FBS, 100 μM β-mercaptoethanol, 2 mM L-glutamine, 0.1 mM nonessential amino acids, 1 mM sodium pyruvate, 50 μg/ml penicillin/streptomycin in Knockout DMEM (Invitrogen) supplemented with 1,000 units/ml LIF (Millipore)). The ESCs were cultured 25 passages on MEF feeder cells and karyotyped at passages 7, 14, and 25 using a standard protocol. Passage 4 ESC lines were weaned off the MEF feeder cells for 4 passages in complete GMEM medium and used in all experiments except karyotyping.

Antibodies, protein immunoblots, immunofluorescence, and AP staining

For protein immunoblots, whole-cell lysates were prepared by treating the cells with modified RIPA buffer [50 mM Tris pH8.0, 150 mM NaCl, 1% NP-40, 0.5% deoxycholic acid, 0.1% SDS, 1x Protease Inhibitors Cocktail (Roche), 10 μg/ml DNaseI (Sigma)] followed by boiling for 15 min. The primary antibodies used are listed in Table S7. Anti-mouse IgG HRP (Pierce), anti-rabbit IgG HRP (Pierce), anti-goat IgG HRP (Jackson ImmunoResearch), and anti-chicken IgY HRP (Jackson ImmunoResearch) were used as secondary antibodies. All protein immunoblot analyses were repeated at least twice and similar results were obtained. For immunofluorescence, ESCs were fixed in 4.0% paraformaldehyde in PBS for 10 min at room temperature, permeabilized twice with 0.4% Triton X-100 in PBS for 10 min each time in PBS, blocked with 4% BSA in PBS for 30 min and stained overnight at 4^oC with the indicated primary antibodies. Anti-rabbit IgG Alexa-Fluor 488 (Invitrogen), anti-mouse IgG Alexa-Fluor 594 (Invitrogen) and anti-chicken IgY Alexa-Fluor 647 (Invitrogen) were used as secondary antibodies. DNA was stained with 1 μg/mL Hoechst 33258 dye (Sigma). For alkaline phosphatase (AP) staining, ESCs were plated at 5.0×10^5 cells per well in a 6-well plate. After incubation at 37^oC for 24 hr, the cells were stained with an Alkaline phosphatase detection kit (Millipore, SCR004) according to the manufacturer's recommendations.

Microscopy

The images from immunofluorescence stained cells were obtained using a Leica SP5 confocal microscope with the same exposure times and processed identically using Adobe Photoshop software. For electron microscopy, trypsinized ESCs were fixed with glutaraldehyde, postfixed with Osmium tetroxide (OsO_4), dehydrated, and embedded in epoxy resin. The embedded specimens were sectioned, stained with uranyl acetate-lead citrate (U-Pb), and images were obtained with an FEI T12 transmission electron microscope equipped with a Gatan digital camera.

Cell proliferation assay

For the MTT assay, wild-type and lamin-null ESCs were plated at 4×10^3 cells per well in a 96-well plate and analyzed 24, 48, 72, 96, 120 and 144 hours after plating. At the indicated time points, ESC medium was replaced with 100 μl 1 mg/ml MTT (3-(4,5-dimethylthiazol-2-yl)-2,5-diphenyltetrazolium bromide, Millipore) in DMEM. After incubation at 37^o C for 3 hours, the MTT solution was removed, and 100 μl DMSO was added to dissolve the formazan precipitate. Absorbance was measured at 570 nm using a Spectramax M5 microplate reader (Molecular Devices). The MTT assay was confirmed by direct counting of live cells as follows. ESCs were plated at 3.5×10^4 cells/cm^2 in a 24-well plate and counted 1, 2, 3, and 5 days after plating. At the indicated time points, ESCs were stained with trypan blue dye and the number of live cells was determined with a hemocytometer. The cell proliferation assays were performed in triplicate at the indicated time points.

RNA extraction and reverse transcriptase PCR

Total RNA was extracted from ESCs, wild-type MEF, or wild-type mouse testis using an RNeasy Plus mini kit (Qiagen). cDNA was reverse transcribed from total RNA with the iScript cDNA synthesis kit (Bio-Rad). To examine the transcription of lamin genes, the indicated exon regions of each lamin gene were amplified from the cDNA by PCR and the amplified PCR products were analyzed using 1.2% agarose gels. The PCR primers were designed to amplify two adjacent exon regions, which are too long to be amplified from the genomic DNA in the PCR conditions used, as follows:

Lmnb1 exon 2-3 (209 bp PCR fragment)
5'-GCGGCACTAAACTCTAAGGATG-3'
5'-TTACGAAACTCCAAGTCCTCAG-3'

Lmnb1 exon 10-11 (201 bp PCR fragment)
5'-CTTCAAGACCACCATACCCG-3'
5'-GAGAAGGCTCTGCACTGTATAC-3'

Lmnb2 exon 2-3 (193 bp PCR fragment)
5'-GTGGCATCAAGACCCTGTAC-3'
5'-GATTCCAGATCCTTCACTCGG-3'

Lmnb2 exon 11-12 (193 bp PCR fragment)

5’-AAGAGGAGGAAGAGGAAGAGG-3’
5’-ACAGTCATCGAGAAACAGACC-3’

Lmna exon 5-6 (205 bp PCR fragment)
5’-AGTCTCGAATCCGCATTGAC-3’
5’-AGCTCCTGGTACTCGTCC-3’

Lmnb3 specific transcript (194 bp PCR fragment)
5’-GGGGAGTCGGAATCCATGAGA-3’
5’-GCCCCCTCTGACTTCACAG-3’

Gapdh exon 5-6 (205 bp PCR fragment)
5’-CTGAACGGGAAGCTCACTG-3’
5’-AGTGGGAGTTGCTGTTGAAG-3’

Generation of Cdx2-CreER2 wild-type or lamin-null ESCs

ESC lines carrying tamoxifen-inducible Cdx2 were obtained according to an established protocol (*24*) with modifications. 8 μg of SalI linearized *pCAG-Cdx2ER-IP*, which is a gift from Dr. H. Niwa, was transfected into ESCs in a 60 mm culture dish using Lipofectamine 2000 (Invitrogen). ESC clones that stably expressed the transgene were selected by growing with 1 μg/ml of puromycin for 8 days. Two independent cell lines for $Lmnb1^{+/+}Lmnb2^{+/+}$ and $Lmnb1^{-/-}Lmnb2^{-/-}$ in which *pCAG-Cdx2ER-IP* was randomly integrated into the genome were used for the gene expression assays. To induce differentiation toward TE cells, the established ESC lines cultured in the absence of tamoxifen were subcultured at 1.2 x 10^4 cells/cm^2 in a culture dish containing 30% TS medium, 70% FCM, 100 nM FGF4, 1 μg/ml heparin and 1 μg/ml 4-hydroxy-tamoxifen (Tx; Sigma). The cells were cultured under this TS condition for 2 days without changing media. TE cells were differentiated from the TS state cells by culturing in 100% TS medium for an additional 6 days, changing media every 2 days. For protein immunoblotting and quantitative real-time PCR analysis, cells were harvested at the indicated time points.

Quantitative real-time PCR analysis of pluripotency and TE genes

Total RNA and cDNA were prepared as described above at the indicated time points. Real-time PCR reaction was done using iQ™ SYBR® Green Supermix (Bio-Rad) and a DNA Engine Opticon Real-Time cycler (MJ Research). The primer sets used are listed in Table S6. The amount of Gapdh expression was used to normalize all values.

Global gene expression analysis

The two independent ESC lines for $Lmnb1^{+/+}Lmnb2^{+/+}$ and $Lmnb1^{-/-}Lmnb2^{-/-}$ that carry *pCAG-Cdx2ER-IP* were used to compare the global gene expression in the pluripotent state. For TE cells, the ES cell lines were differentiated for 8 days as described above. 2.5μg of total RNA extracted with Trizol (Invitrogen) were amplified and labeled by a Low RNA Input Fluorescent Linear Amplification kit (Agilent). The labeled samples were hybridized to the Mouse Developmental Microarray 44k version 3 (developed in the Minoru Ko lab and manufactured by Agilent Technologies, #015087)

(*30*). All target RNAs were labeled with Cy3-CTP and hybridized together with Cy5-CTP labeled reference targets, which are a mixture of Stratagene Universal Mouse Reference RNA and RNA from MC1 cells. Slides were scanned on an Agilent DNA Microarray Scanner, using standard settings, including automatic PMT adjustment. Data from each array were first dye-normalized using Agilent Feature Extraction software, and then the set of all arrays was normalized by the intensity of reference targets as follows: $x' = x - y + \text{average}(y)$, where x and y are $\log_{10}$ intensities of the experimental and reference samples (i.e., Cy3- and Cy5-labeled), respectively, and average(y) is estimated for all arrays. For statistical analysis we used NIA Array Analysis, which performs analysis of variance (ANOVA) on log-transformed intensity values and estimates the False Discovery Rate (FDR) to account for multiple hypothesis testing (*31*). The effect of lamin-B knockout was measured as a log ratio (i.e., difference between means of log-transformed intensities) between lamin-B null and control cells. We considered gene expression change as significant if the log ratio was significantly different from zero (FDR < 0.05) and the change of expression was >2 fold. All microarray data are available at GEO/NCBI (GEO accession: GSE24532, http://www.ncbi.nlm.nih.gov/geo/).

Histology

For histology of E12.5 and E15.5 embryos, whole embryos were dissected from uterine horns, fixed in Bouin's reagent (EMS, 26367-01), dehydrated in a series of diluted ethanol solutions (30% ~ 100%) and 100% xylene, embedded in paraffin, and sagittally sectioned at 10 μm thickness. For E18.5, embryos were kept in ice-cold PBS until soaking in fixative to prevent lung inflation by breathing. After heads were removed for more efficient infiltration, the remaining parts of bodies (torsos) were used for histology. Sectioned embryos were deparaffinized in xylene, rehydrated in serially diluted ethanol solutions (100% - 75%), rinsed with tap water, stained with Gill II haematoxylin (Surgipath, 01522) for 4 min, washed with tap water, treated with Scott's tap water substitute (Surgipath, 02900) for 10 - 15 s until the staining color turned blue, washed with tap water, stained with eosin (Surgipath, 01602) for 30 s, destained in 95% ethanol, followed by 100% ethanol, xylene, then mounted in Permount (Fisher Scientific, SP15-100) with a coverslip. For phrenic nerve staining of E18.5 diaphragms, sectioned torsos were deparaffinized and boiled in antigen retrieval solution (Dako, S1699) for 10 min, blocked with 10% donkey serum in PBST (0.1% Triton-X 100 in PBS) for 30 min, and incubated with mouse anti-neurofilament antibody (DSHB, 2H3, 1:50) overnight at 4°C, and detected with a Vector ABC kit (Vector Laboratories) followed by a DAB substrate kit (Vector Laboratories) according to the manufacturer's recommendations. Detailed protocols for fixation and embedding available upon request.

Brain analyses

E14.5, E15.5 and E18.5 mouse brains were dissected, fixed in 4% paraformaldehyde in PBS at 4°C either for 2 hrs (E14.5 and E15.5) or for 4 hrs (E18.5), cryoprotected by soaking in 30% sucrose in PBS at 4°C overnight, embedded in tissue freezing medium (Triangle Biomedical), and frozen on dry ice. Frozen brains were coronally sectioned at 14 or 20 μm thickness with a Leica CM3050S cryostat. For E9.5, whole embryos were fixed for 2 hrs, cryoprotected overnight, embedded in freezing medium, frozen on dry ice and sagittally sectioned at 14 μm thickness. Sections were

boiled in antigen retrieval solution (Dako, S1699) for 10 min, blocked with 10% donkey serum in PBST for 30 min, and incubated with primary antibodies overnight at 4°C. The primary antibodies used for brain analyses are listed in Table S7. The secondary antibodies used were anti-rabbit Alexa Fluor 488, anti-goat Alexa Fluor 555 (Invitrogen, 1:500), anti-mouse DyLight 488, anti-rabbit DyLight 594 and anti-goat DyLight 647 (Jackson ImmunoResearch, 1:1000). DNA was counterstained with 1 μg/ml Hoechst 33258 dye for 10 min. Images were obtained using a Leica SP5 confocal microscope and processed as described in the Microscopy section. For Nissl staining of E18.5 mouse brain, frozen sections were defatted at room temperature in ethanol/chloroform (1:1) overnight, rehydrated in a series of ethanol dilution and incubated in 0.1% cresyl violet at 55°C for 10 min. For analysis of spindle orientation, frozen sections were immunostained with anti-Pericentrin, anti-Nestin and Hoechst dye. The angle of the mitotic cleavage plane of anaphase cells relative to the surface plane of the ventricular zone was measured from confocal images. To measure relative cell cycle length and exit rate, BrdU was dissolved in PBS at 5 mg/ml and injected intraperitoneally at 50 μg/g body weight into pregnant mothers at E14.5. The injected mothers were euthanized at 30 min or 24 hr after injection to determine cell cycle length or exit rate, respectively. Embryos were kept on ice-cold PBS until the brain dissection of an entire litter was complete. For the neuronal birth dating assay, BrdU was injected at E14.5 and mothers were euthanized at E18.5.

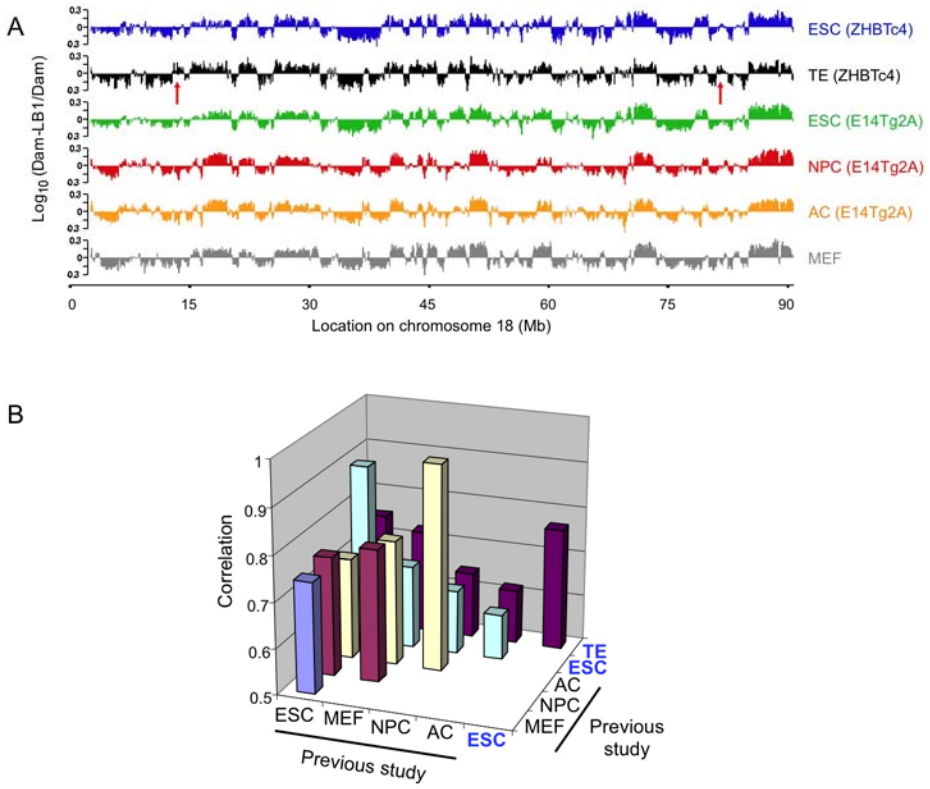

Fig. S1. Analyses of patterns of lamin-B1 binding among different cell lines. (A) Lamin-B1 binding profiles on mouse chromosome 18. Profiles determined in this study for ZHBTc4 ESCs (blue) and TE cells (black, differentiated from ZHBTc4) are compared to those determined in a previous study with E14Tg2A ESCs (green), neural progenitor cells (NPC, red, differentiated from E14Tg2A), astrocytes (AC, orange, differentiated from E14Tg2A), or mouse embryonic fibroblasts (MEF, grey). Y-axis, the intensity of lamin-B1 binding plotted as the average $\log_{10}$ ratio of methylation values of Dam-lamin-B1 over Dam alone at 100-Kb intervals. Data for E14Tg2A ESC, NPC, AC, and MEF were obtained from the GEO database (GSE17051) and converted to the same scale and intervals as in this study. Red arrows indicate examples of lamin-B1-binding regions in TE cells that are different from all the other cells. (B) Comparisons were made between lamin-B1 and chromatin interactions in ESCs and TE cells mapped in this study (labeled in blue letters) with the previously reported maps in a different ESC line and its differentiated neuronal lineage cells, the neuronal progenitor cell (NPC) and astrocytes (AS). A high correlation of lamin-B1 and chromatin binding was found between the two different ESCs used in the two studies (correlation values of median Dam-ID log-ratio at 100Kb intervals, r = 0.893 ± 0.004 SE). However lamin-B1-binding patterns of TE cells differed from ESCs (r = 0.750 ± 0.004), fibroblasts (r = 0.725 ± 0.004), neural progenitor cells (r = 0.644 ± 0.004), and astrocytes (r = 0.617 ± 0.004).

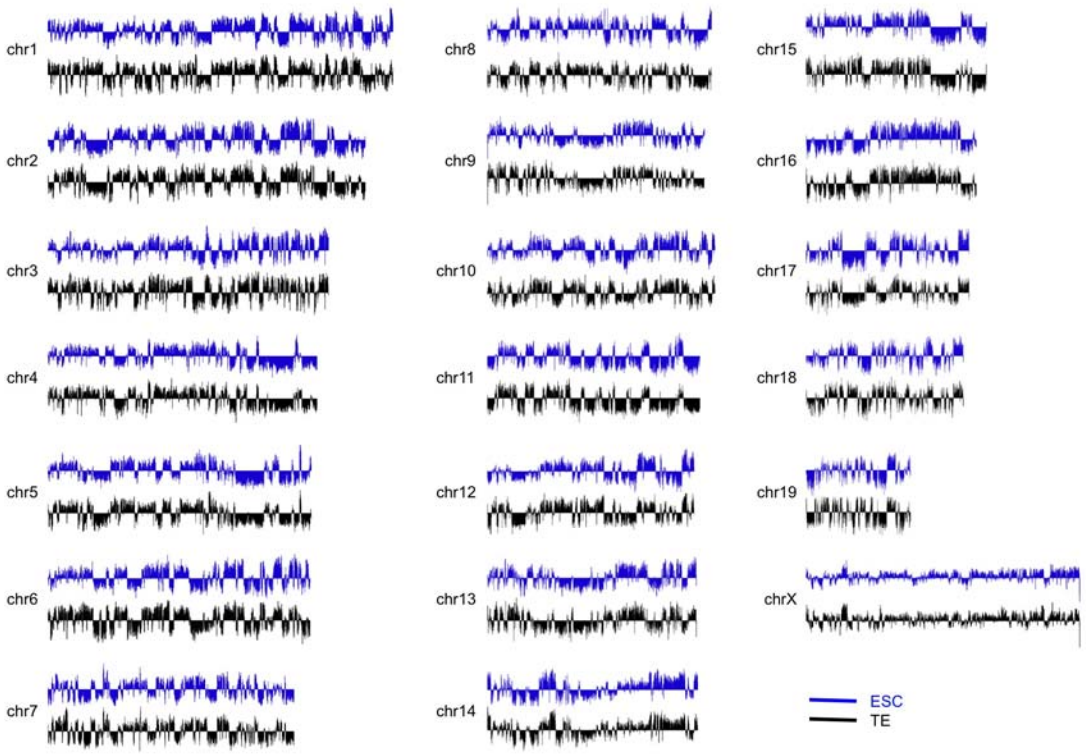

Fig. S2. Patterns of lamin-B1 and chromatin interactions in ZHBTc4 ESCs (blue) and TE cells differentiated from ZHBTc4 (black) of each chromosome. Although the overall patterns are similar between the two cell types, many differences are apparent in local areas along each of the chromosomes.

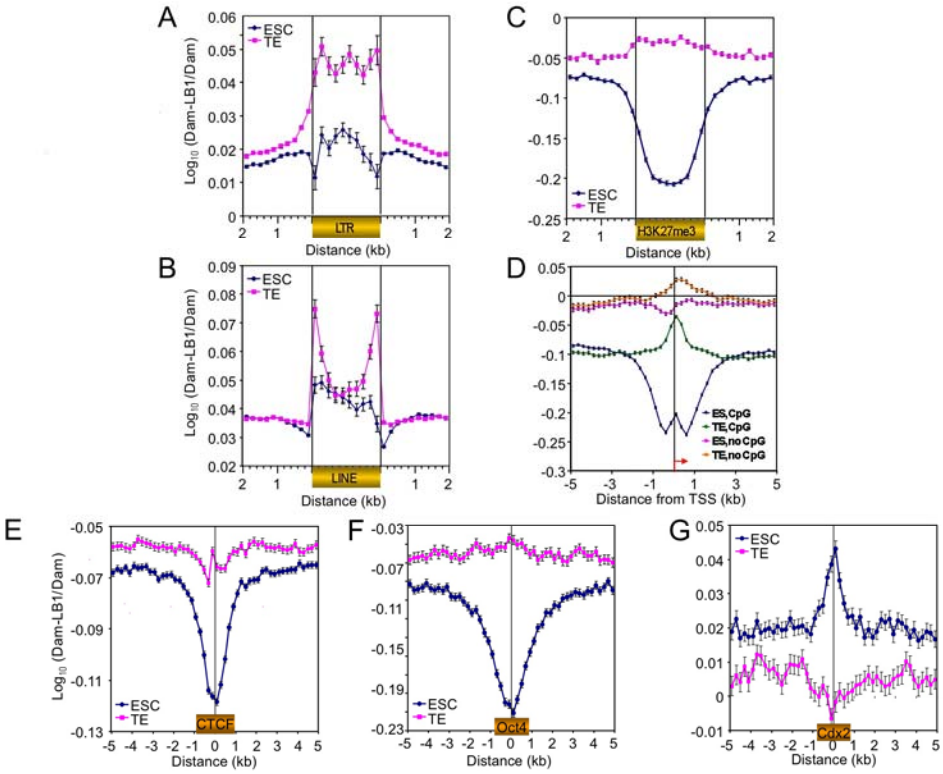

Fig. S3. Fine scale (0.5 to 2-Kb intervals) analyses of lamin-B1 binding to different genomic elements in ESCs (blue) and TE cells (magenta). (A) Lamin-B1 binding at Long terminal repeats (LTRs) in ESCs and TE cells. The relative binding increases as ESCs differentiate into TE cells. (B) Lamin-B1 binding at Long interspersed nuclear elements (LINEs) in ESCs and TE cells. Note the sharp drop of relative binding at the boundaries of the LINEs, while the relative binding increases as ESCs differentiate into TE cells. (C) The relative interaction between lamin-B1 and chromatin at chromatin regions containing histone H3K27 trimethylation marks (H3K27me3) in ESCs and TE cells (*32*). The relative binding increases as ESCs differentiate into TE cells. (D) The relative average binding of lamin-B1 to promoters with or without CpG islands. The red arrow indicates the transcriptional start site (TSS). Genes containing CpG islands exhibit a relative increase in lamin-B1 binding to their promoters as ESCs (blue) differentiate into TE cells (green). Genes lacking CpG islands generally exhibit relatively higher lamin-B1 binding than those containing CpG islands in both ESCs (magenta) and TE cells (orange). There is a small relative increase of lamin-B1 binding in the genes without CpG islands as ESCs differentiate into the TE cells. In general, genes with CpG islands that were silenced in TE cells have more lamin-B1 binding than those that were expressed. (E) The binding of lamin-B1 to the regions near the binding sites for transcription factor CTCF increases as ESCs differentiate toward the TE cells. (F) The relative binding of lamin-B1 to regions near the binding sites for transcription factor Oct4, a gene essential for pluripotency which decreases during differentiation, increases as ESCs differentiate into TE cells. (G) The relative binding of lamin-B1 to regions near

the binding sites for transcription factor Cdx2, a gene essential for TE differentiation and is increased in TE cells, decreases as ESCs differentiate into TE cells.

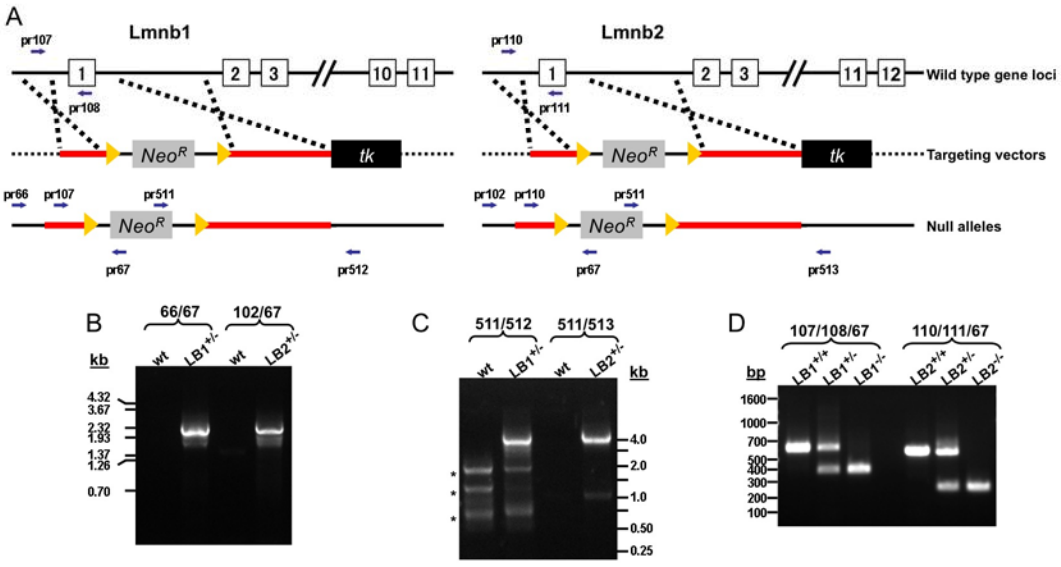

Fig. S4. Analyses of *Lmnb1* and *Lmnb2* targeting in mice. (A) Diagrams of the targeting strategy. The 1.16 Kb and 1.54 Kb proximal promoter regions *(33, 34)* and the first exons (exons are indicated as squares with the corresponding exon numbers, black line represents the promoter or intronic regions) in *Lmnb1* and *Lmnb2* genes, respectively, were deleted using the targeting vectors shown. Vector construction can be found in the Supplementary Material. Red lines represent the targeting arms corresponding to the genomic regions in the *Lmnb* genes. Yellow arrows represent the loxP sites. Neo^R, neomycin resistance gene. TK, thymidine kinase gene. (B and C) Confirmation of homologous recombination of the 5' (B) and 3' (C) arms in *Lmnb1* and *Lmnb2* genes. The locations of PCR primers are indicated in A. The primer sequences and expected PCR fragment sizes are listed in the Supplementary Materials and Methods. Correct homologous recombination of the 5' and 3' arms is indicated by the amplification of ~2.3 Kb and ~4.4 Kb PCR fragments, respectively, in both the *Lmnb1* ($LB1^{+/-}$) and *Lmnb2* ($LB2^{+/-}$) heterozygous mice. Asterisks mark nonspecific bands. (D) Genotyping strategies of lamin-B knockout mice. A set of three PCR primers as indicated in A were used to amplify the wild-type ($LB1^{+/+}$ or $LB2^{+/+}$), *Lmnb1* or *Lmnb2* heterozygous ($LB1^{+/-}$ or $LB2^{+/-}$) or null ($LB1^{-/-}$ or $LB2^{-/-}$) alleles.

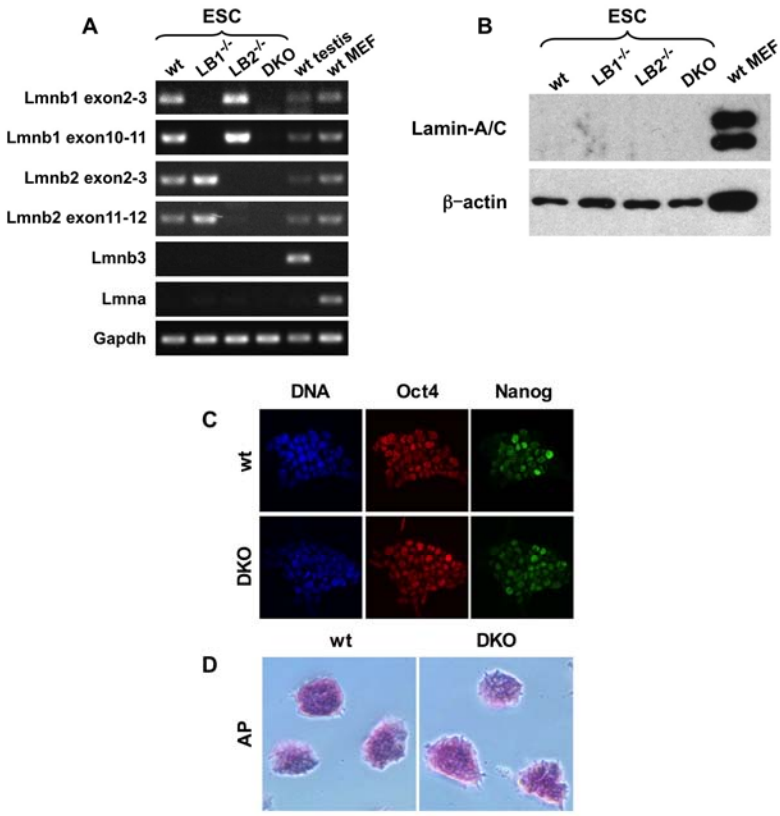

Fig. S5. Analysis of *Lmnb1*$^{-/-}$*Lmnb2*$^{-/-}$ ESCs. (A) Verification of *Lmnb1*$^{-/-}$*Lmnb2*$^{-/-}$ ESCs using reverse transcriptase (RT) PCR. RT-PCR was performed using RNA prepared from the *Lmnb1*$^{+/+}$*Lmnb2*$^{+/+}$ (wt), *Lmnb1*$^{-/-}$*Lmnb2*$^{+/+}$ (LB1$^{-/-}$), *Lmnb1*$^{+/+}$*Lmnb2*$^{-/-}$ (LB2$^{-/-}$), and *Lmnb1*$^{-/-}$*Lmnb2*$^{-/-}$ (DKO) ESCs. The primer sequences and expected PCR fragment sizes are listed in the Supplementary Materials and Methods. Similar results were obtained from two biological repeats. (B) Protein immunoblotting analyses of lamin-A and lamin-C. Wild-type MEF lysates were used as positive controls for lamin-A and lamin-C. β-actin was used as a loading control. (C) Immunofluorescence staining of ESCs with antibodies to Oct4 and Nanog. DNA was counterstained with Hoechst dye. (D) Alkaline phosphatase (AP) staining of ESCs.

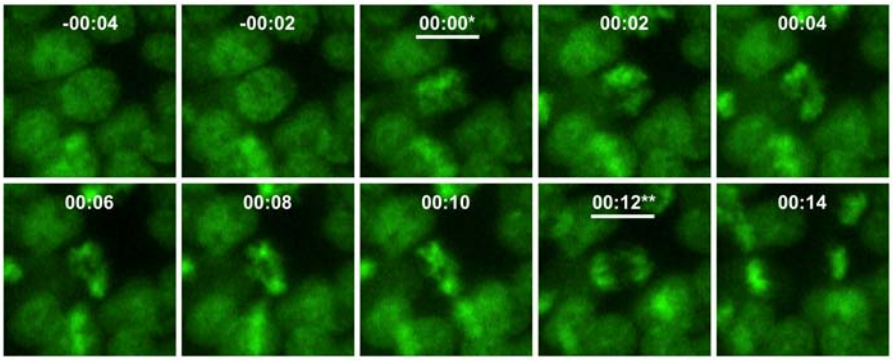

Fig. S6. Time-lapse images of histone H2B-GFP expressing *Lmnb1*$^{-/-}$*Lmnb2*$^{-/-}$ ESCs during mitosis. The images were acquired at 2 min intervals. The time elapsed from the first sign of nuclear envelope break down (NEBD, time 00:00 underlined) to the first frame of chromosome separation as indicated by the splitting of the metaphase chromosomes into two sets of anaphase chromosomes (time 00:12 underlined) was determined. Although *Lmnb1*$^{-/-}$*Lmnb2*$^{-/-}$ ESCs take slightly longer to proceed from NEBD to anaphase onset (1-2 min) than *Lmnb1*$^{+/+}$*Lmnb2*$^{+/+}$ ESCs, we did not observe a significant change in the overall cell cycle length as judged by time elapsed from one anaphase to the next anaphase.

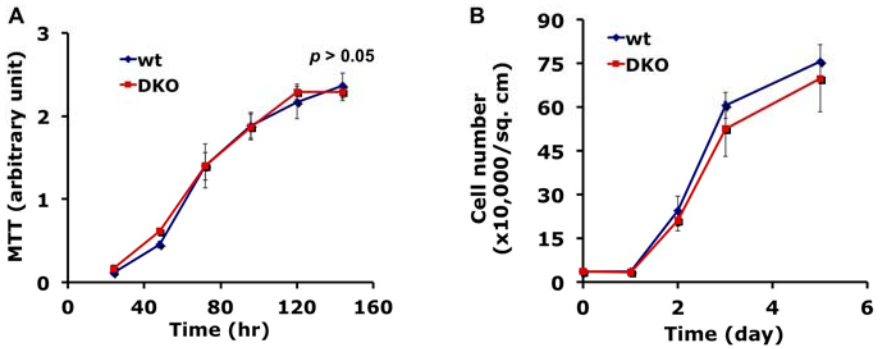

Fig. S7. Analyses of cell proliferation of *Lmnb1*$^{+/+}$*Lmnb2*$^{+/+}$ and *Lmnb1*$^{-/-}$*Lmnb2*$^{-/-}$ ESCs. (A) The growth curves of ESCs as determined by the MTT proliferation assay, which measures the enzyme activity that reduces MTT (3-(4,5-dimethylthiazol-2-yl)-2,5-diphenyltetrazolium bromide) to formazan dye. (B) The number of viable ESCs determined by the absence of trypan blue staining was counted at the indicated days in culture. The *Lmnb1*$^{+/+}$*Lmnb2*$^{+/+}$ and *Lmnb1*$^{-/-}$*Lmnb2*$^{-/-}$ ESCs exhibit similar proliferation rates. Error bars, standard deviation (SD, N = 3).

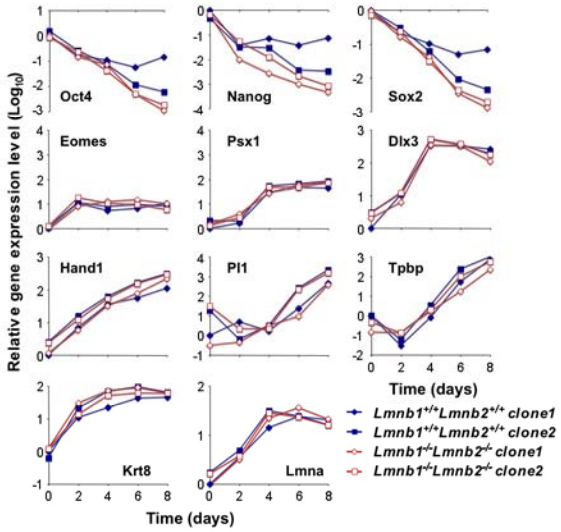

Fig. S8. Measurements of expression of genes encoding selected ESC and TE markers, and lamin-A & lamin-C using q-PCR as ESCs differentiated into the TE lineage. Two different ESC clones for *Lmnb1*$^{+/+}$*Lmnb2*$^{+/+}$ and *Lmnb1*$^{-/-}$*Lmnb2*$^{-/-}$ were used. All values were normalized by GAPDH amounts.

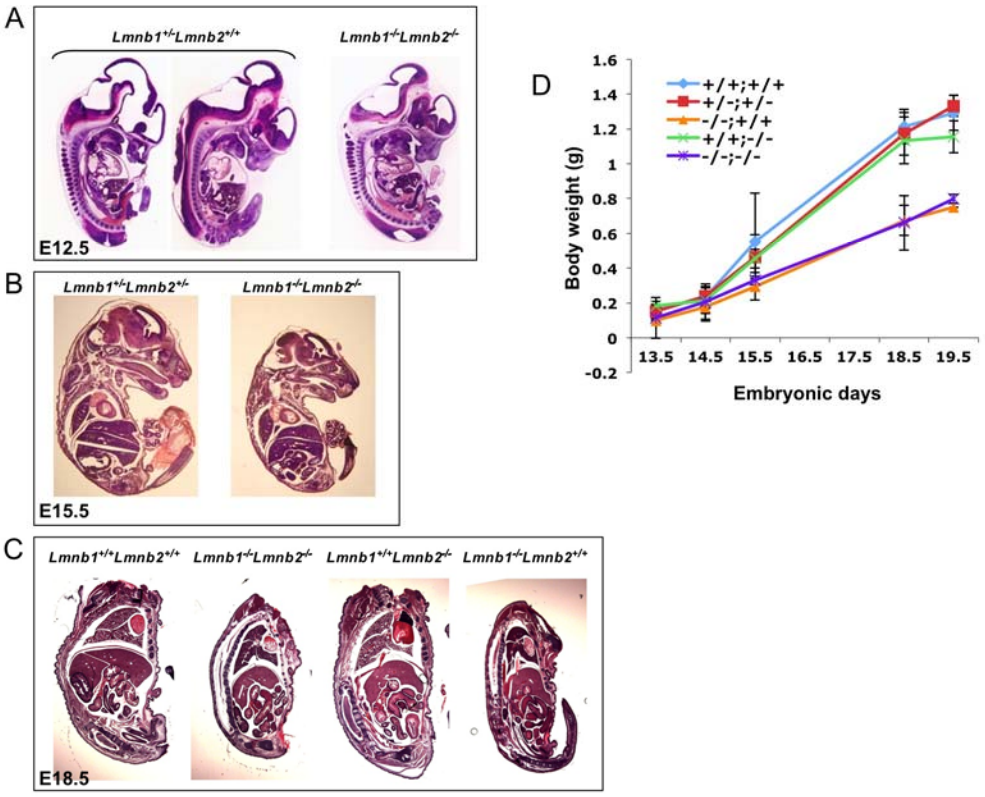

Fig. S9. Analysis of gross embryo morphology and measurement of body weights of lamin-B mutant embryos. (A-C) H & E staining of sagittal sections of E12.5, E15.5, and E18.5 embryos. The heads of the E18.5 embryos were removed for more efficient penetration of fixatives and stains. All internal organs are present. (D) The body weight of embryos from E13.5-E19.5 of different genotypes. Note that body sizes of *Lmnb1*$^{-/-}$ *Lmnb2*$^{-/-}$ embryos appeared smaller from E14-15, and by E18.5 these mice at 0.66 ± 0.15 g were significantly smaller than *Lmnb1*$^{+/+}$*Lmnb2*$^{+/+}$ mice at 1.21 ± 0.09 g (T-test, $p < 10^{-5}$, N = 7). *Lmnb1*$^{-/-}$*Lmnb2*$^{+/+}$ mice were also smaller (0.67 ± 0.08 g, T-test, $p < 10^{-6}$, N = 7), whereas *Lmnb1*$^{+/+}$*Lmnb2*$^{-/-}$ mice (1.13 ± 0.13 g) were similar in size as *Lmnb1*$^{+/+}$*Lmnb2*$^{+/+}$ littermates. Error bars, standard error of the mean (SEM). +/+;+/+, *Lmnb1*$^{+/+}$*Lmnb2*$^{+/+}$; +/-;+/-, *Lmnb1*$^{+/-}$*Lmnb2*$^{+/-}$; -/-;+/+, *Lmnb1*$^{-/-}$*Lmnb2*$^{+/+}$; +/+;-/-, *Lmnb1*$^{+/+}$*Lmnb2*$^{-/-}$; -/-;-/-, *Lmnb1*$^{-/-}$*Lmnb2*$^{-/-}$.

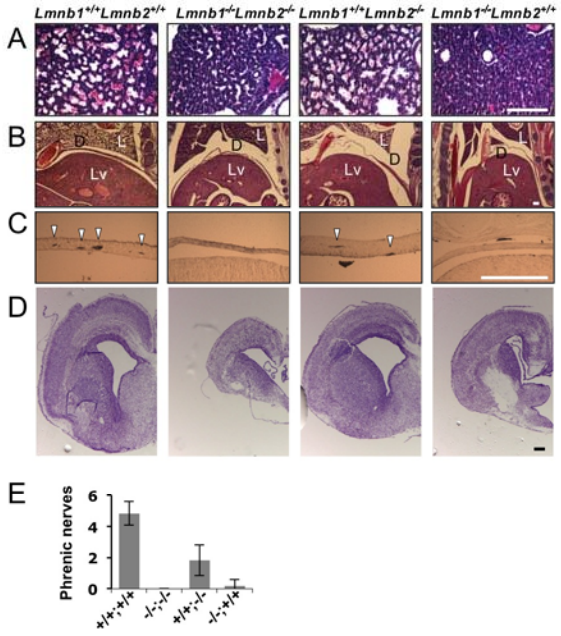

Fig. S10. Requirements for lamin-Bs in development of the lung, diaphragm, and brain. (A-D) Analyses of E18.5 embryonic tissues. Genotypes are indicated above the images. (A) Representative images of lung tissues stained with H & E at E18.5. (B) Regions of diaphragms of lamin-B mutants appear thin and wavy compared to those of the wild-type littermate. L, lung; D, diaphragm; Lv, liver. (C) Representative images of diaphragms stained with anti-neurofilament (NF) antibody at E18.5. Arrowheads indicate phrenic nerve bundles. (D) Nissl staining of coronal sections of the neocortex at low magnification. (E) Quantification of phrenic nerve bundles. Error bars, SD; n = 6. +/+;+/+, *Lmnb1*$^{+/+}$*Lmnb2*$^{+/+}$; -/-;-/-, *Lmnb1*$^{-/-}$*Lmnb2*$^{-/-}$; +/+;-/-, *Lmnb1*$^{+/+}$*Lmnb2*$^{-/-}$; -/-;+/+, *Lmnb1*$^{-/-}$*Lmnb2*$^{+/+}$ in E. Scale bars, 200 μm.

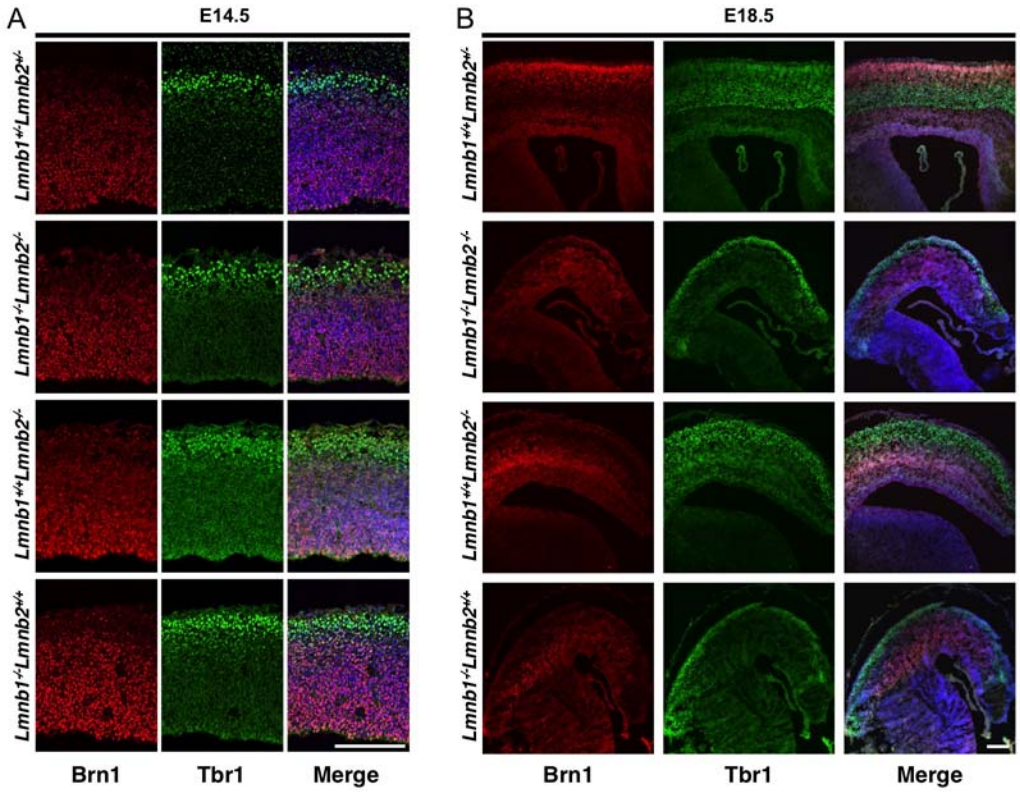

Fig. S11. The relative positions of Tbr1- and Brn1- positive neuronal layers are the same at E14.5 (A) but reversed at E18.5 (B) in all lamin-B mutant neocortices compared to those in the control littermates. Scale bars, 200 μm.

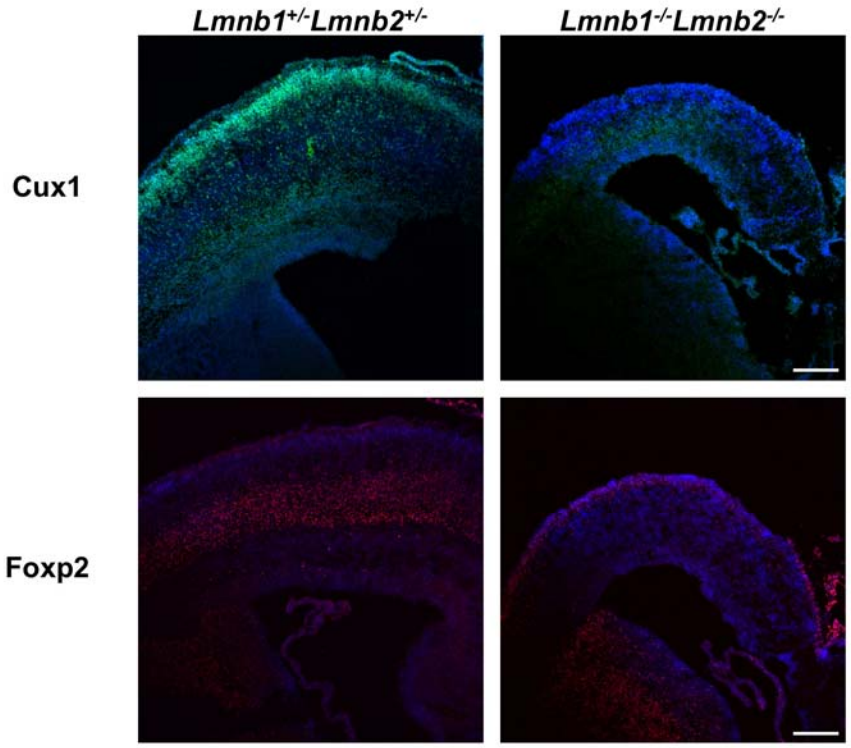

Fig. S12. Disorganization of various neuronal cells in the brains of the E18.5 *Lmnb1*$^{-/-}$ *Lmnb2*$^{-/-}$ mice as judged by immunostaining of Foxp2 and Cux1, which label neurons in the early-born deep-layer (VI and subplate) and the late-born outer layers (II-IV) of the neocortex, respectively. Scale bars, 200 μm.

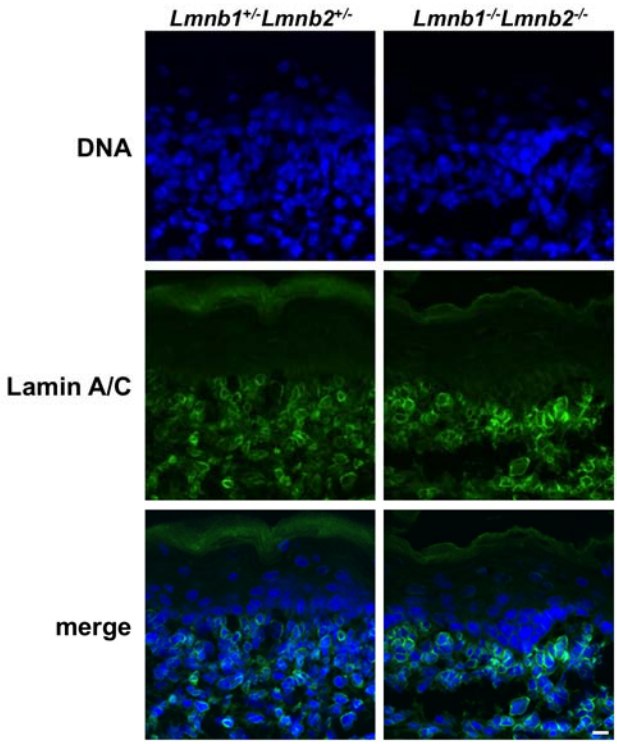

Fig. S13. A-type lamins are present in the hind limb skin of E18.5 embryos. A-type lamins are strongly expressed in dermal cells, which contrasts with little or no expression in epidermal cells (*35*). Both *Lmnb1*$^{-/-}$*Lmnb2*$^{-/-}$ and *Lmnb1*$^{+/-}$*Lmnb2*$^{+/-}$ mice exhibit similar A-type lamin staining patterns in the skin cells. Although our antibodies detected lamin-A where it is expressed, we did not detect A-type lamins in all tested embryonic brain sections (data not shown). This supports the previous report that lamin-A is not expressed in the embryonic brains (*4*). Detection of lamin-A staining at the peripheries of *Lmnb1*$^{-/-}$*Lmnb2*$^{-/-}$ dermal cell nuclei suggests that B-types are not required for proper localization of A-type lamins. Scale bars, 10 μm.

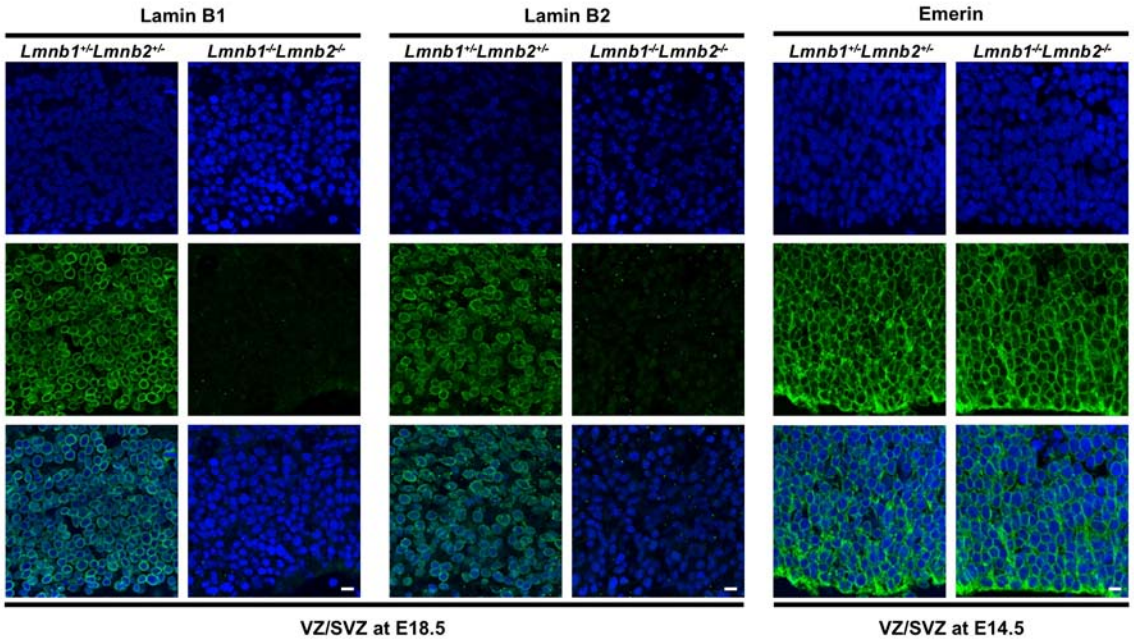

Fig. S14. *Lmnb1*$^{-/-}$*Lmnb2*$^{-/-}$ mice lack B-type lamins, but exhibit similar nuclear morphology (except for the presence of more pyknotic nuclei that are undergoing apoptosis) and emerin staining in the neocortex as the *Lmnb1*$^{+/-}$*Lmnb2*$^{+/-}$ littermates. Shown are ventricular (VZ)/subventricular (SVZ) zones with indicated genotypes stained with anti-lamin-B1, -B2, and -emerin antibodies (green). Nuclei were stained with Hoechst dye (blue). Scale bars, 10 μm.

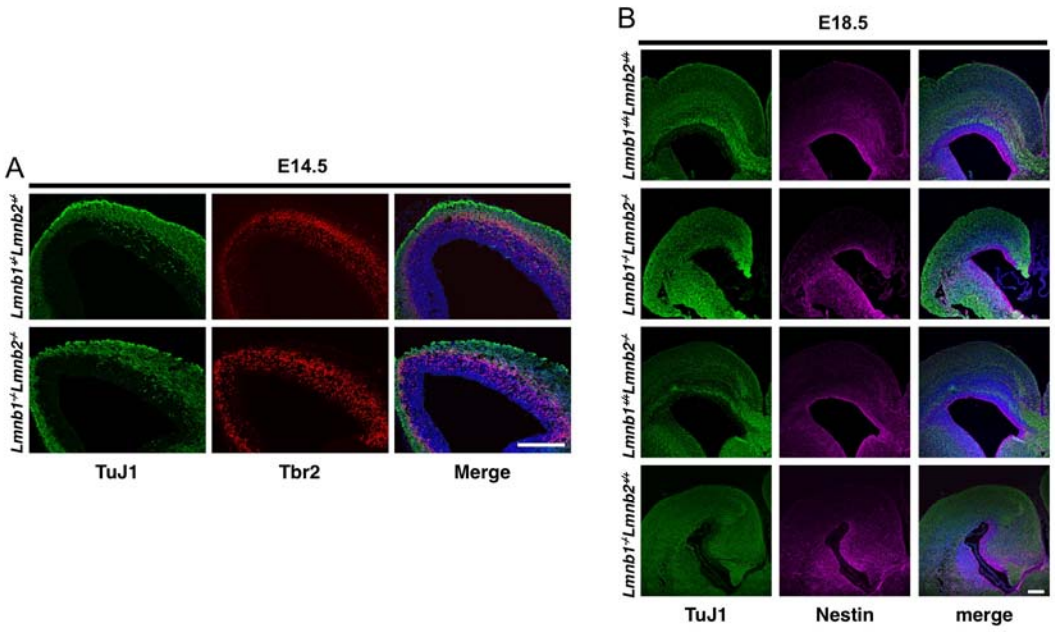

Fig. S15. Relative position and thickness of differentiated neuronal cells and neural progenitor cell layers in the neocortex are largely maintained at both E14.5 (A) and E18.5 (B) in lamin-B mutants as judged by immunostaining of TuJ1 (green), Tbr2 (red), and Nestin (magenta), which label differentiated neurons, intermediate (or basal) progenitor, and neural progenitor cells in the cortex, respectively. Most TuJ1 positive cells do not localize beyond the basal side of Tbr2 layer in both control and lamin-B mutant cortices, indicating no premature neuronal differentiation at the subventricular zone. Scale bars, 200 μm.

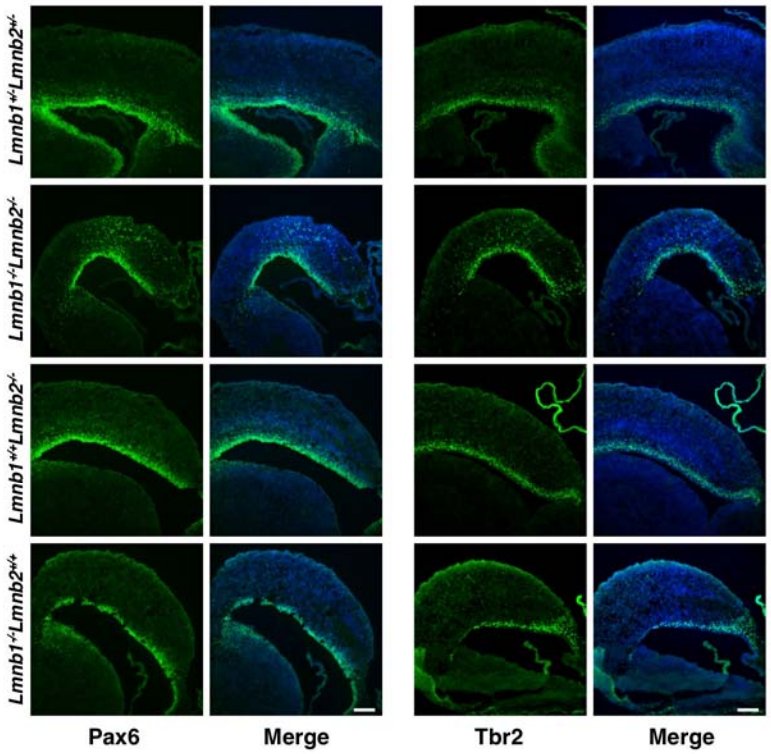

Fig. S16. Pax6- and Tbr2-positive progenitor cells normally found in VZ and SVZ, respectively, are scattered into cortical regions of the neocortex in E18.5 *Lmnb1*$^{-/-}$*Lmnb2*$^{-/-}$ mice, but not in *Lmnb1*$^{-/-}$*Lmnb2*$^{+/+}$, *Lmnb1*$^{+/+}$*Lmnb2*$^{-/-}$ or control littermates. Scale bars, 200 μm.

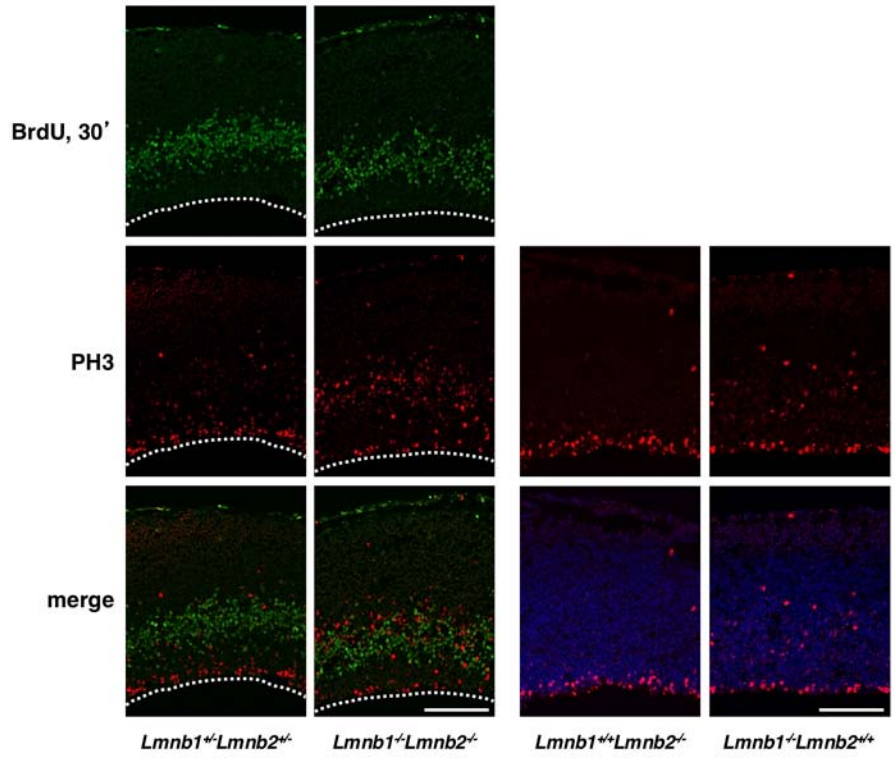

Fig. S17. Altered localization of mitotic cells in the neocortex of *Lmnb1*$^{-/-}$*Lmnb2*$^{-/-}$ mice at E14.5. Pulse BrdU-labeling (30') marked S-phase cells and phospho-Histone H3 (PH3) marked G2/M phase cells. In *Lmnb1*$^{+/-}$*Lmnb2*$^{+/-}$, *Lmnb1*$^{-/-}$*Lmnb2*$^{+/+}$ and *Lmnb1*$^{+/+}$*Lmnb2*$^{-/-}$ mice, PH3+ cells are mainly localized at the apical surface of VZ, whereas the PH3+ cells are scattered into the basal side of VZ in the *Lmnb1*$^{-/-}$*Lmnb2*$^{-/-}$ cortex. Scale bars, 100 μm.

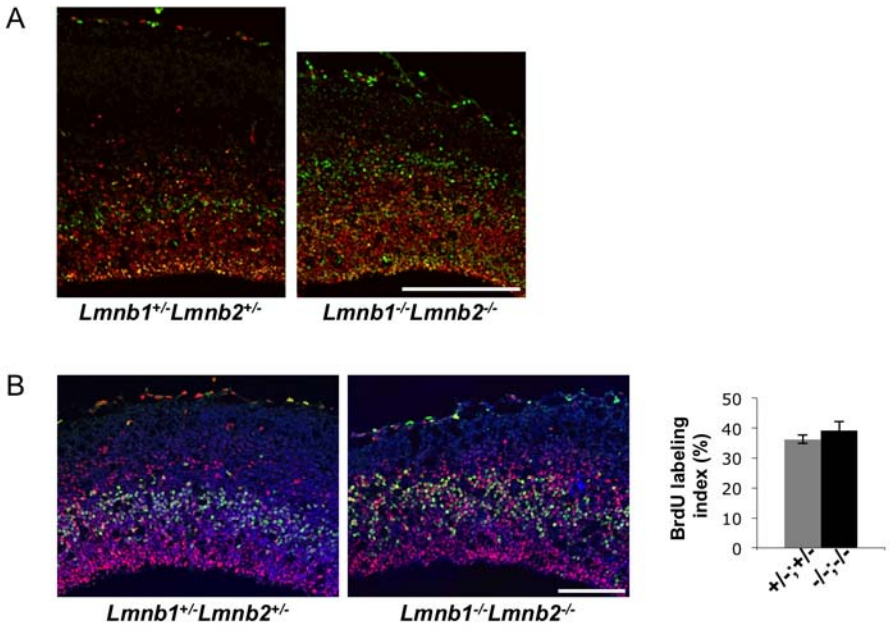

Fig. S18. (A) Representative images for measuring cell cycle exit rates shown in Fig. 4H. (B) Cell cycle lengths of proliferating cells in VZ/SVZ of the neocortex were analyzed in *Lmnb1*$^{+/-}$*Lmnb2*$^{+/-}$ and *Lmnb1*$^{-/-}$*Lmnb2*$^{-/-}$ brains. BrdU was injected 30' before dissection to pulse label S-phase cells of the E14.5 embryos. BrdU labeling index is calculated by dividing the number of BrdU+ cells (green, S phase) by the number of Ki67+ cells (red, all proliferating cells). The similar BrdU indices indicate that cells of both genotypes are cycling at a similar rate. Error bars, SEM. T-test, $p > 0.05$, N = 9 sections (> 60 cells per section). +/-;+/-, *Lmnb1*$^{+/-}$*Lmnb2*$^{+/-}$; -/-;-/-, *Lmnb1*$^{-/-}$*Lmnb2*$^{-/-}$.

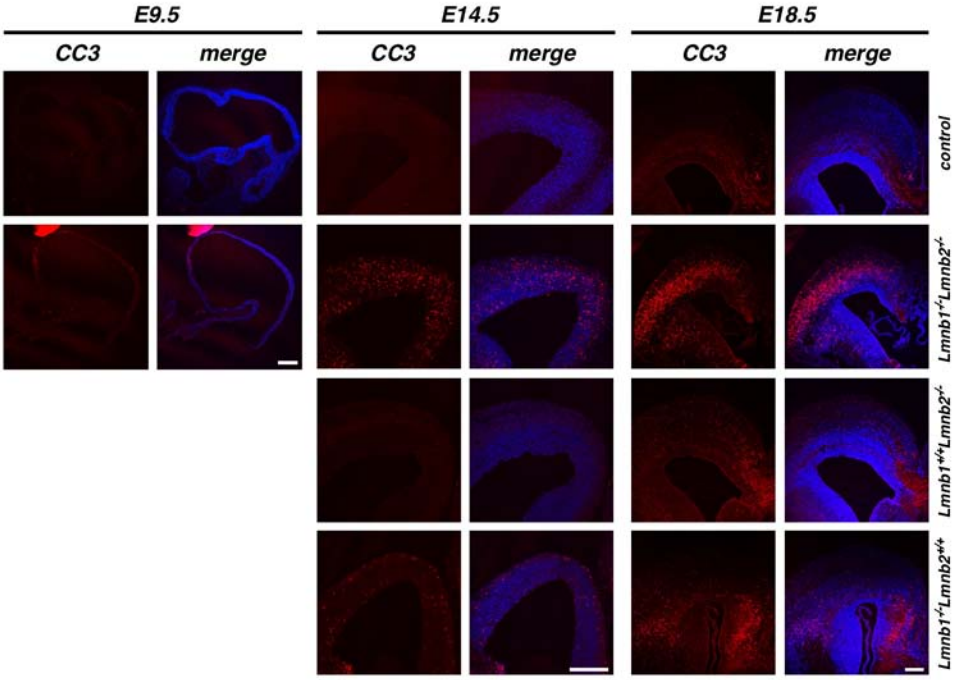

Fig. S19. Analyses of apoptosis. Increased apoptosis was detected in *Lmnb1*$^{-/-}$*Lmnb2*$^{-/-}$ brains as early as E9.5. Sagittal sections of E9.5 embryos and coronal sections of E14.5 and E18.5 neocortices were stained with anti-CC3 (cleaved caspase 3, red) and Hoechst dye (blue). Apoptotic cells were detected in the neocortex of *Lmnb1*$^{-/-}$*Lmnb2*$^{+/+}$ mice at E14.5, and by E18.5 more cells underwent apoptosis. In *Lmnb1*$^{+/+}$*Lmnb2*$^{-/-}$ mice, no apparent apoptosis was detected at E14.5 but clear apoptosis was observed at E18.5. Scale bars, 200 μm.

Table S1. Lamin-B1 binding to promoters of genes in mouse ESCs and TE cells (see the separate Excel file). Because the major difference in lamin-B1 binding appeared within 2 kb from the transcription start site (TSS), we used this region to estimate the relative amounts of lamin-B1 interaction with individual genes.

P7		P14		P25	
DKO	wt	DKO	wt	DKO	wt
40	40	40	40	39	40
40	40	39	39	40	40
40	40	40	40	40	42
39	40	40	40	40	39
40	40	40	40	40	40
40	41	40	40	40	40
40	40	40	40	41	40
40	40	40	40	40	40
40	41	40	40	40	41
40	40	40	40	39	40
39	40	40	40	40	40
40	40	40	40	40	39
40	39	40	39	40	39
40	40	40	40	40	40
39	40	40	40	40	40
40	40	40	40	40	40
40	40	40	41	40	40
40	40	39	40	40	40
40	40	40	40	40	40
40	39	40	40	40	40
40	40	40	40	39	40
40	40	40	40	40	40
40	40	39	41	40	40
42	39	40	40	40	40
40	40	40	40	40	40
40	40	39	40	39	40
40	40	40	40	40	40
40	41	40	41	40	40
40	39	39	40	40	41
40	40	40	40	41	40
euploid cells (%)	86.7	76.7	83.3	83.3	80.0	80.0

Table S2. Karyotyping analyses of *Lmnb1*$^{-/-}$*Lmnb2*$^{-/-}$ (DKO) and *LmnB1*$^{+/+}$*LmnB2*$^{+/+}$ (wt) ESCs that had been cultured for the indicated number of passages. The karyotype number was determined by analyzing 30 different cells in each genotype and passage. The percentage of correct karyotypes (euploid cells) are similar between the two types of ESCs.

Featureid	Mean expression (DKO ESC)	Mean experession (wt ESC)	LogRatio	FoldChnge	P	FDR	Symbol	Annotation
Z00070209-1	1.1513	2.805	-1.6537	45.05	0	0	Afm	afamin
Z00048585-1	0.9392	2.2465	-1.3073	20.29	0	0	9430027B09Rik	RIKEN cDNA 9430027B09 gene
Z00075211-1	2.3183	3.5646	-1.2463	17.631	0	0	Lmnb1	lamin B1
Z00056538-1	3.5862	4.64229	-1.05609	11.378	0	0	Lmnb2	lamin B2
Z00040250-1	1.2842	2.1471	-0.8629	7.292	0	0.006	Speer5-ps1	spermatogenesis associated glutamate (E)-rich protein 5, pseudogene 1
Z00030203-1	2.1571	2.9937	-0.8366	6.864	0	0.0013	2010012P19Rik	RIKEN cDNA 2010012P19 gene
Z00052917-1	1.2435	2.0585	-0.815	6.531	0	0.0247	AI593442	expressed sequence AI593442
Z00056200-1	3.9827	4.7944	-0.8117	6.481	0	0	LOC384710	similar to Acidic ribosomal phosphoprotein P0
Z00045784-1	2.3895	3.1955	-0.806	6.397	0	0.0287	Aox3	aldehyde oxidase 3
Z00024504-1	0.9308	1.7048	-0.774	5.942	0	0.0294	Itih3	inter-alpha trypsin inhibitor, heavy chain 3
Z00029804-1	1.8665	2.6232	-0.7567	5.71	0	0.0008	LOC433082	hypothetical gene supported by AK086736
Z00074920-1	1.9144	2.6122	-0.6978	4.986	0	0.0138	Usp44	ubiquitin specific peptidase 44
Z00055724-1	0.8479	1.5381	-0.6902	4.9	0	0.0166	Slamf7	SLAM family member 7
Z00026675-1	0.7632	1.4277	-0.6645	4.618	0	0.012	V1ra5	vomeronasal 1 receptor, A5
Z00025626-1	0.7609	1.4093	-0.6484	4.45	0	0.0004	Papln	papilin, proteoglycan-like sulfated glycoprotein
Z00011924-1	1.5676	2.19189	-0.62429	4.21	0	0.0418	Akr1c19	aldo-keto reductase family 1, member C19
Z00026050-1	0.6829	1.2675	-0.5846	3.842	0	0.0001	D130017N08Rik	RIKEN cDNA D130017N08 gene
Z00062638-1	0.8283	1.3424	-0.5141	3.266	0	0.0013	4933432I03Rik	RIKEN cDNA 4933432I03 gene
Z00054362-1	0.8283	1.33759	-0.50929	3.23	0	0.0113	BC034902	cDNA sequence BC034902
Z00075718-1	0.845	1.3486	-0.5036	3.188	0	0.0433	Evi2a	ecotropic viral integration site 2a
Z00023175-1	0.8176	1.3156	-0.498	3.147	0	0.006	Gpr88	G-protein coupled receptor 88
Z00038798-1	0.8353	1.3221	-0.4868	3.067	0	0.0131	LOC670300	hypothetical protein LOC670300
Z00022182-1	2.6012	3.0756	-0.4744	2.981	0	0.0008	9130213B05Rik	RIKEN cDNA 9130213B05 gene
Z00023841-1	0.854	1.3182	-0.4642	2.912	0	0.0138	Pcdhb4	protocadherin beta 4
Z00062155-1	0.7392	1.1898	-0.4506	2.822	0	0.023	4930435H24Rik	RIKEN cDNA 4930435H24 gene
Z00061043-1	0.7771	1.225	-0.4479	2.804	0	0.0199	9930111H07Rik	RIKEN cDNA 9930111H07 gene
Z00025304-1	0.8081	1.25269	-0.44459	2.783	0	0.012	Mefv	Mediterranean fever
Z00076124-1	0.8817	1.32309	-0.44139	2.763	0	0.012	F630111L10Rik	RIKEN cDNA F630111L10 gene
Z00026228-1	0.9098	1.33879	-0.42899	2.685	0	0.0175	Pcdhb6	protocadherin beta 6
Z00032773-1	0.8338	1.26279	-0.42899	2.685	0	0.0166	Ifne1	interferon epsilon 1
Z00058004-1	2.3654	2.7505	-0.3851	2.427	0	0.0287	LOC638533	similar to serine (or cysteine) proteinase inhibitor, clade B, member 9b
Z00011952-1	3.2807	3.6612	-0.3805	2.401	0	0.0247	2510049I19Rik	RIKEN cDNA 2510049I19 gene
Z00035652-1	3.2822	2.82391	0.45829	2.872	0	0.0247	Txnl4a	thioredoxin-like 4A
Z00022894-1	5.0593	4.5813	0.478	3.006	0	0.0004	Erdr1	erythroid differentiation regulator 1
Z00063211-1	2.758	2.1289	0.6291	4.256	0	0.0085	9330159M07Rik	RIKEN cDNA 9330159M07 gene
Z00063059-1	2.6437	2.01331	0.63039	4.269	0	0.005	Peg13	paternally expressed 13
Z00061581-1	2.8862	2.2519	0.6343	4.308	0	0.0166	B230206L02Rik	RIKEN cDNA B230206L02 gene
Z00024242-1	1.5919	0.9234	0.6685	4.661	0.0001	0.0473	Gpr143	G protein-coupled receptor 143
Z00023088-1	2.5438	1.8569	0.6869	4.862	0	0.0002	Chgb	chromogranin B
Z00031835-1	3.337	2.6237	0.7133	5.167	0	0	Apoa2	apolipoprotein A-II
Z00031578-1	2.1635	1.4475	0.716	5.199	0	0.0047	3110045C21Rik	RIKEN cDNA 3110045C21 gene
Z00004620-1	3.2366	2.507	0.7296	5.365	0	0.0001	6230416J20Rik	RIKEN cDNA 6230416J20 gene
Z00075607-1	1.6437	0.90301	0.74069	5.504	0.0001	0.0473	3830402I07Rik	RIKEN cDNA 3830402I07 gene
Z00033422-1	2.3479	1.5937	0.7542	5.678	0	0.019	Vmn2r-ps105	vomeronasal 2, receptor, pseudogene 105
Z00070225-1	2.6802	1.9257	0.7545	5.681	0	0	Atg4c	autophagy-related 4C (yeast)
Z00036400-1	1.8051	1.0125	0.7926	6.202	0	0.0323	Srd5a1	steroid 5 alpha-reductase 1
Z00024060-1	2.2762	1.44931	0.82689	6.712	0	0.0087	Crisp1	cysteine-rich secretory protein 1
Z00037910-1	1.8076	0.978	0.8296	6.754	0	0.019	Ccdc38	coiled-coil domain containing 38
Z00043329-1	2.4578	1.5284	0.9294	8.499	0	0	LOC14210	hypothetical LOC14210
Z00071747-1	3.6553	2.6944	0.9609	9.139	0	0	LOC227506	similar to Lta4h protein
Z00055038-1	3.7795	2.794	0.9855	9.671	0	0.0009	Hal	histidine ammonia lyase
Z00017768-1	3.7036	2.69661	1.00699	10.162	0	0	Nod1	nucleotide-binding oligomerization domain containing 1
Z00012780-1	2.9937	1.7627	1.231	17.021	0	0.0001	6030458C11Rik	RIKEN cDNA 6030458C11 gene
Z00076367-1	3.6357	1.6529	1.9828	96.116	0	0	BC005512	cDNA sequence BC005512

Table S3. A list of differentially expressed genes between the *LmnB1*$^{+/+}$*LmnB2*$^{+/+}$ (wt) and *Lmnb1*$^{-/-}$*Lmnb2*$^{-/-}$ (DKO) ESCs as determined by microarray analyses.

Featureid	Mean expression (DKO TE)	Mean experession (wt TE)	LogRatio	FoldChng	P	FDR	Symbol	Annotation
Z00048585-1	1.4528	3.17039	-1.71759	52.19	0	0	9430027B09Rik	RIKEN cDNA 9430027B09 gene
Z00070347-1	0.9884	2.1876	-1.1992	15.819	0	0.0057	Gdap7	ganglioside-induced differentiation-associated-protein 7
Z00026204-1	1.4364	2.5696	-1.1332	13.589	0	0.0493	4930515G01Rik	RIKEN cDNA 4930515G01 gene
Z00075211-1	2.1295	3.24409	-1.11459	13.019	0	0	Lmnb1	lamin B1
Z00070209-1	1.8545	2.90629	-1.05179	11.266	0	0.0208	Afm	afamin
Z00062986-1	1.2692	2.31009	-1.04089	10.987	0	0	0610039H22Rik	RIKEN cDNA 0610039H22 gene
Z00009742-1	0.7556	1.6828	-0.9272	8.456	0	0.0042	Ccdc90a	coiled-coil domain containing 90A
Z00070094-1	0.8371	1.6513	-0.8142	6.519	0	0.0396	4930524O07Rik	RIKEN cDNA 4930524O07 gene
Z00056200-1	3.8688	4.6664	-0.7976	6.274	0	0	LOC384710	similar to Acidic ribosomal phosphoprotein P0
Z00056538-1	3.1095	3.90609	-0.79659	6.26	0	0	Lmnb2	lamin B2
Z00030687-1	1.8993	2.5308	-0.6315	4.28	0	0.0242	Nr2f1	nuclear receptor subfamily 2, group F, member 1
Z00026107-1	2.3821	3.0121	-0.63	4.265	0	0.0126	Nnmt	nicotinamide N-methyltransferase
Z00022894-1	5.2228	4.7533	0.4695	2.947	0	0.0008	Erdr1	erythroid differentiation regulator 1
Z00078186-1	2.4487	1.9529	0.4958	3.131	0	0.0494	C130098C10Rik	RIKEN cDNA C130098C10 gene
Z00039222-1	2.7017	2.1372	0.5645	3.668	0	0.0181	Zbtx	zinc finger, B-box domain containing
Z00050099-1	1.1517	0.56521	0.58649	3.859	0	0.0449	Arl11	ADP-ribosylation factor-like 11
Z00074160-1	2.8309	2.2098	0.6211	4.179	0	0.0015	Myo15b	myosin XVB
Z00004620-1	2.6601	1.96751	0.69259	4.927	0	0.0004	6230416J20Rik	RIKEN cDNA 6230416J20 gene
Z00076367-1	2.8002	2.0178	0.7824	6.058	0	0.0004	BC005512	cDNA sequence BC005512
Z00070225-1	3.0343	2.22211	0.81219	6.489	0	0	Atg4c	autophagy-related 4C (yeast)
Z00043578-1	1.8002	0.9871	0.8131	6.502	0	0.0009	Arhgef15	Rho guanine nucleotide exchange factor (GEF) 15
Z00059373-1	1.7738	0.9254	0.8484	7.053	0	0.0149	LOC632779	similar to Spindlin-like protein 2 (SPIN-2)
Z00031578-1	2.4467	1.58451	0.86219	7.28	0	0	3110045C21Rik	RIKEN cDNA 3110045C21 gene
Z00043329-1	2.0028	1.1059	0.8969	7.886	0	0	LOC14210	hypothetical LOC14210
Z00071747-1	3.4276	2.5035	0.9241	8.396	0	0	LOC227506	similar to Lta4h protein
Z00024225-1	2.8151	1.8578	0.9573	9.063	0	0.0002	Cyct	cytochrome c, testis
Z00075607-1	2.0173	0.9095	1.1078	12.817	0	0	3830402I07Rik	RIKEN cDNA 3830402I07 gene
Z00063059-1	3.073	1.8284	1.2446	17.563	0	0	Peg13	paternally expressed 13

Table S4. A list of differentially expressed genes in *Lmnb1*$^{+/+}$*Lmnb2*$^{+/+}$ (wt) and *Lmnb1*$^{-/-}$ *Lmnb2*$^{-/-}$ (DKO) TE cells that were derived from the corresponding ESCs in Table S3 as determined by microarray analyses.

Lmnb1	Lmnb2	Embryos		Expected ratio (%)
		E12.5	E18.5	
+/+	+/+	2 (4.3*)	22 (9.5)	6.3
+/+	+/-	3 (6.5)	39 (16.8)	12.5
+/+	-/-	2 (4.3)	13 (5.6)	6.3
+/-	+/+	6 (13.0)	20 (8.6)	12.5
+/-	+/-	13 (28.3)	56 (24.1)	25.0
+/-	-/-	6 (13.0)	27 (11.6)	12.5
-/-	+/+	4 (8.7)	13 (5.6)	6.3
-/-	+/-	8 (17.4)	28 (12.1)	12.5
-/-	-/-	2 (4.3)	14 (6.0)	6.3
total		46 (100)	232 (100)	100.0

** observed ratio*

Table S5. Analyses of progenies from *Lmnb1*$^{+/-}$*Lmnb2*$^{+/-}$ intercrosses. The lamin-B genotypes of the embryonic day 12.5 (E12.5) and 18.5 (E18.5) embryos are indicated at left. The numbers of live E12.5 and E18.5 embryos are indicated. The observed ratio for each genotype is shown in parentheses, while the expected ratio is in the column at right. *Lmnb1*$^{-/-}$*Lmnb2*$^{-/-}$, *Lmnb1*$^{-/-}$*Lmnb2*$^{+/+}$, and *Lmnb1*$^{+/+}$*Lmnb2*$^{-/-}$ mice were born but died immediately thereafter.

gene	forward primer	reverse primer
Oct4	5'-CTCCCGAGGAGTCCCAGGACAT-3'	5'-GATGGTGGTCTGGCTGAACACCT-3'
Nanog	5'-CAAGGGTCTGCTACTGAGATGCTCTG-3'	5'-TTTTGTTTGGGACTGGTAGAAGAATCAG-3'
Sox2	5'-CGAGATAAACATGGCAATCAAATG-3'	5'-AACGTTTGCCTTAAACAAGACCAC-3'
Eomes	5'-CCTGGTGGTGTTTTGTTGTG-3'	5'-TTTAATAGCACCGGGCACTC-3'
Psx1	5'-GAATTGGTTTCGGATGAGGA-3'	5'-GTGGCTCAGAAGAAGCCATC-3'
Dlx3	5'-GCCTTAGGGGTAAGGCTGTC-3'	5'-GACCTGCTTCTCTTGGTTGC-3'
Hand1	5'-CCCCTCTTCCGTCCTCTTAC-3'	5'-CTGCGAGTGGTCACACTGAT-3'
Pl1	5'-TACCCTGCTTGGTCTGGACT-3'	5'-GGGCACTCAACATTCGTTCT-3'
Tpbp	5'-AAGTTAGGCAACGAGCGAAA-3'	5'-AGTGCAGGATCCCACTTGTC-3'
Krt8	5'-TTCTGATGTCGTGTCCAAGTG-3'	5'-TCTCTAGTTCCCTGCACTCTG-3'
Lmna	5'-GGAAGTCGATGAAGAGGGAAAG-3'	5'-TTTAGGGTGAACTTCGGTGG-3'
Gapdh	5'-CTTTGTCAAGCTCATTTCCTGG-3'	5'-TCTTGCTCAGTGTCCTTGC-3'

Table S6. A list of primer sets used for quantitative real-time PCR analyses of gene expression in ESCs and TE cells.

Name	Antigen	Host organism	Source	Dilution	WB/IF/IHC
lamin B (C-20)	lamin B1	goat, poly	Santa Cruz, sc-6216	1:200	WB/IF
lamin B2 (E3)	lamin B2	mouse, mono	Invitrogen, 332100	1:500	WB/IF
LB2 (C-6164)	lamin B2	chicken, poly	raised in this study	1:10,000	IF
lamin A (N-18)	lamin A/C	goat, poly	Santa Cruz, sc-6215	1:100	WB
133A2	lamin A/C	mouse, mono	Abcam, ab8980	1:100	IF
AC40	beta-actin	mouse, mono	Sigma, A3853	1:2,000	WB
Oct-3/4 (C-10)	Pou5f1	mouse, mono	Santa Cruz, sc-5279	1:2,000	WB/IF
Nanog	Nanog	rabbit, poly	Abcam, ab14959	1:5,000	WB/IF
Sox2	Sox2	rabbit, poly	Abcam, ab15830	1:500	WB
Cytokeratin 8	Krt 8	mouse, mono	Santa Cruz, sc-101459	1:200	WB
Gapdh (FL-335)	Gapdh	rabbit, poly	Santa Cruz, sc-25778	1:1,000	WB
2H3	neurofilament	mouse, mono	DSHB	1:50	IHC
Tbr1	Tbr1	rabbit	Abcam, ab31940	1:200	IF
Brn1	Brn1	mouse	Novus, H00005455-A01	1:100	IF
M8	pericentrin	rabbit, poly	raised in lab	1:400	IF
Rat-401	nestin	mouse, mono	BD pharmingen, 556309	1:200	IF
nestin (R-20)	nestin	goat, poly	Santa Cruz, sc-21249	1:200	IF
BU-33	BrdU	mouse, mono	Sigma, B2531	1:50	IF
Ki67	MKI67	rabbit, poly	Abcam, ab15580	1:1,000	IF
CC3	cleaved caspase3	rabbit, mono	Cell signaling, 9664	1:200	IF
emerin (FL-254)	emerin	rabbit, poly	Santa Cruz, sc-15378	1:100	IF
CDP (M-22)	CDP (Cux1)	rabbit, poly	Santa Cruz, sc-13024	1:250	IF
Foxp2	Foxp2	goat	Santa Cruz	1:500	IF
TuJ1	Tubulin beta III	mouse, mono	Covance, MMS-435P	1:200	IF
Tbr2/Eomes	Tbr2/Eomes	rabbit, poly	Abcam, ab23345	1:200	IF
Pax6	Pax6	rabbit, poly	Millipore, AB2237	1:500	IF
PH3 (ser10)	PH3 (ser10)	rabbit, poly	Millipore, 09-797	1:200	IF

Table S7. A list of antibodies, their sources, hosts, and dilutions used for protein immunoblotting (WB), immunofluorescence (IF), and immunohistochemistry (IHC).

References for Supplementary Material

1. T. Dechat *et al.*, Nuclear lamins: major factors in the structural organization and function of the nucleus and chromatin. *Genes Dev* **22**, 832 (Apr 1, 2008).
2. T. V. Cohen, C. L. Stewart, Fraying at the edge mouse models of diseases resulting from defects at the nuclear periphery. *Curr Top Dev Biol* **84**, 351 (2008).
3. C. Stewart, B. Burke, Teratocarcinoma stem cells and early mouse embryos contain only a single major lamin polypeptide closely resembling lamin B. *Cell* **51**, 383 (Nov 6, 1987).
4. R. A. Rober, K. Weber, M. Osborn, Differential timing of nuclear lamin A/C expression in the various organs of the mouse embryo and the young animal: a developmental study. *Development* **105**, 365 (Feb, 1989).
5. Y. Zheng, A membranous spindle matrix orchestrates cell division. *Nat Rev Mol Cell Biol* **11**, 529 (Jul, 2010).
6. M. Y. Tsai *et al.*, A mitotic lamin B matrix induced by RanGTP required for spindle assembly. *Science* **311**, 1887 (Mar 31, 2006).
7. L. Ma *et al.*, Requirement for Nudel and dynein for assembly of the lamin B spindle matrix. *Nat Cell Biol* **11**, 247 (Mar, 2009).
8. B. Goodman *et al.*, Lamin-B3 counteracts the kinesin Eg5 to restrain spindle pole separation during spindle assembly. *J Biol Chem* **285**, 35238 (Sep, 2010).
9. R. I. Kumaran, D. L. Spector, A genetic locus targeted to the nuclear periphery in living cells maintains its transcriptional competence. *J Cell Biol* **180**, 51 (Jan 14, 2008).
10. L. E. Finlan *et al.*, Recruitment to the nuclear periphery can alter expression of genes in human cells. *PLoS Genet* **4**, e1000039 (Mar, 2008).
11. C. Lanctot, T. Cheutin, M. Cremer, G. Cavalli, T. Cremer, Dynamic genome architecture in the nuclear space: regulation of gene expression in three dimensions. *Nat Rev Genet* **8**, 104 (Feb, 2007).
12. J. Kind, B. van Steensel, Genome-nuclear lamina interactions and gene regulation. *Curr Opin Cell Biol* **22**, 320 (Jun, 2010).
13. K. L. Reddy, J. M. Zullo, E. Bertolino, H. Singh, Transcriptional repression mediated by repositioning of genes to the nuclear lamina. *Nature* **452**, 243 (Mar 13, 2008).
14. L. Guelen *et al.*, Domain organization of human chromosomes revealed by mapping of nuclear lamina interactions. *Nature* **453**, 948 (Jun 12, 2008).
15. D. Peric-Hupkes *et al.*, Molecular maps of the reorganization of genome-nuclear lamina interactions during differentiation. *Mol Cell* **38**, 603 (May, 2010).
16. J. Liu *et al.*, Essential roles for Caenorhabditis elegans lamin gene in nuclear organization, cell cycle progression, and spatial organization of nuclear pore complexes. *Mol Biol Cell* **11**, 3937 (Nov, 2000).
17. S. Osouda *et al.*, Null mutants of Drosophila B-type lamin Dm(0) show aberrant tissue differentiation rather than obvious nuclear shape distortion or specific defects during cell proliferation. *Developmental biology* **284**, 219 (Aug 1, 2005).
18. S. H. Yang *et al.*, An absence of both lamin B1 and lamin B2 in keratinocytes has no effect on cell proliferation or the development of skin and hair. *Hum Mol Genet* **20**, 3537 (Sep 15, 2011).

19. L. Vergnes, M. Peterfy, M. O. Bergo, S. G. Young, K. Reue, Lamin B1 is required for mouse development and nuclear integrity. *Proc Natl Acad Sci U S A* **101**, 10428 (Jul 13, 2004).
20. C. Coffinier *et al.*, Abnormal development of the cerebral cortex and cerebellum in the setting of lamin B2 deficiency. *Proc Natl Acad Sci U S A* **107**, 5076 (Mar 16).
21. H. Niwa, J. Miyazaki, A. G. Smith, Quantitative expression of Oct-3/4 defines differentiation, dedifferentiation or self-renewal of ES cells. *Nat Genet* **24**, 372 (Apr, 2000).
22. N. Cloonan *et al.*, Stem cell transcriptome profiling via massive-scale mRNA sequencing. *Nat Methods* **5**, 613 (Jul, 2008).
23. J. Nichols, J. Silva, M. Roode, A. Smith, Suppression of Erk signalling promotes ground state pluripotency in the mouse embryo. *Development* **136**, 3215 (Oct, 2009).
24. H. Niwa *et al.*, Interaction between Oct3/4 and Cdx2 determines trophectoderm differentiation. *Cell* **123**, 917 (Dec 2, 2005).
25. M. Yamada *et al.*, The essential role of LIS1, NDEL1 and Aurora-A in polarity formation and microtubule organization during neurogensis. *Cell Adh Migr.* **4**, 180 (Apr, 2010).
26. C. Coffinier *et al.*, Deficiencies in lamin B1 and lamin B2 cause neurodevelopmental defects and distinct nuclear shape abnormalities in neurons. *Mol. Biol. Cell* **22**, 4683 (Dec, 2011).
27. J. Quinn, T. Kunath, J. Rossant, Mouse trophoblast stem cells. *Methods Mol Med* **121**, 125 (2006).
28. M. J. Vogel, D. Peric-Hupkes, B. van Steensel, Detection of in vivo protein-DNA interactions using DamID in mammalian cells. *Nat Protoc* **2**, 1467 (2007).
29. C. L. Stewart, Production of chimeras between embryonic stem cells and embryos. *Methods Enzymol* **225**, 823 (1993).
30. M. G. Carter *et al.*, Transcript copy number estimation using a mouse whole-genome oligonucleotide microarray. *Genome Biol* **6**, R61 (2005).
31. A. A. Sharov, D. B. Dudekula, M. S. Ko, A web-based tool for principal component and significance analysis of microarray data. *Bioinformatics* **21**, 2548 (May 15, 2005).
32. T. S. Mikkelsen *et al.*, Genome-wide maps of chromatin state in pluripotent and lineage-committed cells. *Nature* **448**, 553 (Aug 2, 2007).
33. H. Maeno, K. Sugimoto, N. Nakajima, Genomic structure of the mouse gene (Lmnb1) encoding nuclear lamin B1. *Genomics* **30**, 342 (Nov 20, 1995).
34. M. Zewe *et al.*, Gene structure and chromosomal localization of the murine lamin B2 gene. *Eur J Cell Biol* **56**, 342 (Dec, 1991).
35. J. Zhang *et al.*, A human iPSC model of Hutchinson Gilford Progeria reveals vascular smooth muscle and mesenchymal stem cell defects. *Cell Stem Cell* **8**, 31 (Jan 7, 2011).